

Inhomogeneous Big Bang Nucleosynthesis Revisited

Juan F. Lara*

*Department of Physics and Astronomy, Clemson University,
Clemson, South Carolina 29631, USA and
National Astronomical Observatory of Japan,
2-21-1 Osawa, Mitaka, Tokyo 181-8588, Japan*

Toshitaka Kajino†

*National Astronomical Observatory and Graduate University for Advanced Studies,
2-21-1 Osawa, Mitaka, Tokyo 181-8588, Japan and
Department of Astronomy, Graduate School of Science,
University of Tokyo, 7-3-1 Hongo, Bunkyo-ku Tokyo 113-0033, Japan*

Grant J. Mathews‡

*University of Notre Dame, Center for Astrophysics, Notre Dame, IN 46556, USA and
National Astronomical Observatory of Japan,
2-21-1 Osawa, Mitaka, Tokyo 181-8588, Japan*

(Dated: October 13, 2019)

Abstract

We reanalyze the allowed parameters for inhomogeneous big bang nucleosynthesis in light of the WMAP constraints on the baryon-to-photon ratio η and a recent measurement which has set the neutron lifetime to be $878.5 \pm 0.7 \pm 0.3$ seconds. For a set baryon-to-photon ratio η the new lifetime reduces the mass fraction of ^4He by 0.0015 but does not significantly change the abundances of other isotopes. This enlarges the region of concordance between ^4He and deuterium in the parameter space of η and the IBBN distance scale r_i . The ^7Li abundance can be brought into concordance with observed ^4He and deuterium abundances by using depletion factors as high as 9.3. The WMAP constraints, however, severely limit the allowed comoving ($T = 100$ GK) inhomogeneity distance scale to $r_i \approx (1.3 - 2.6) \times 10^5$ cm.

PACS numbers: 26.35.+c

Keywords: Inhomogenous big bang nucleosynthesis, Neutron Lifetime, Cosmic Microwave Background

^{*}Electronic address: ljuan@clemson.edu

[†]Electronic address: kajino@nao.ac.jp

[‡]Electronic address: gmathews@nd.edu

I. INTRODUCTION

Big bang nucleosynthesis (BBN) plays a crucial role in constraining our views on the universe. It is essentially the only probe of physics in the early radiation dominated epoch during the interval from $\sim 1 - 10^4$ sec. Moreover, big bang cosmology is currently undergoing rapid evolution based upon high precision determinations of cosmological parameters and improved input physics. Thus, it is important to scrutinize all possible variants of BBN and understand the constraints which modern observations place upon their parameters. This paper summarizes the current status on one such important variant of the big bang, namely one in which the baryons are spatially inhomogeneously distributed during the epoch of nucleosynthesis. We consider the constraints from *WMAP* and the latest observed elemental abundances and include recent measurements of thermonuclear reaction rates and the neutron lifetime. We show, that although the parameter space for inhomogeneous big bang nucleosynthesis (IBBN) is significantly limited, interesting regions remain and this paradigm continues to be a viable possibility for the early universe.

II. BACKGROUND

At a high temperature in the early universe, e.g. $T \sim 100$ GK (the corresponding age of the universe is ~ 0.01 seconds) baryons mainly exist in the form of free neutrons and protons. During this epoch neutrons and protons are rapidly interconverted via the following weak reactions [1, 2, 3]

$$\begin{aligned} n + \nu_e &\leftrightarrow p + e^- \\ n + e^+ &\leftrightarrow p + \bar{\nu}_e \\ n &\leftrightarrow p + e^- + \bar{\nu}_e. \end{aligned}$$

As long as these reactions are in thermal equilibrium the ratio of neutrons to protons is given by $(n/p) = \exp[-\Delta m/kT]$ where Δm is the mass difference between neutrons and protons. When the universe cools to a temperature $T = 13$ GK these weak reactions fall out of equilibrium. The n/p ratio after that time decreases only due to neutron decay.

When the universe cools to a temperature $T \approx 0.9$ GK the nuclear reaction $n + p \leftrightarrow d + \gamma$ falls out of nuclear statistical equilibrium. Deuterium production becomes significant,

leading to the synthesis of increasingly heavier nuclei through a network of nuclear reactions and weak decays. When nearly all free neutrons are incorporated into ${}^4\text{He}$ nuclei, ${}^4\text{He}$ production virtually stops. The final mass fraction can be approximated as

$$Y_p \approx 2(n/p)/[(n/p) + 1]. \quad (1)$$

Detailed final abundances depend most sensitively on the baryon-to-photon ratio η . Observational measurements of ${}^4\text{He}$, deuterium and ${}^7\text{Li}$ abundances can be compared with abundances calculated from BBN to put constraints on η . Constraints can also be put on η from measurements of the Cosmic Microwave Background (CMB). The physics of acoustic oscillations in the CMB angular power spectrum has a dependence on various cosmological parameters (See Melchiorri [4] for comprehensive references to methods of CMB calculations), including the baryon density factor $\Omega_b h^2$, and therefore η . Recent CMB measurements using *WMAP* [5] set $\Omega_b h^2 = 0.0224 \pm 0.0009$ and $\eta = 6.13 \pm 0.25 \times 10^{-10}$. See Lara [6] for references to previous attempts to constrain η using BBN or the CMB.

The final n/p ratio depends on the neutron lifetime, τ_n , which partially determines when weak reactions fall out of equilibrium. The most recent lifetime world average [7] is $\tau_n = 885.7 \pm 0.8$ seconds. But a recent measurement by Serebrov et al. [8] sets $\tau_n = 878.5 \pm 0.7_{\text{stat}} \pm 0.3_{\text{sys}}$ seconds, which differs from the world average by six standard deviations. Serebrov et al. measured the storage loss rate $\tau_{\text{storage}}^{-1} = \tau_n^{-1} + \tau_{\text{loss}}^{-1}$ of ultracold neutrons in a gravitational trap, and then extrapolated the data down to $\tau_{\text{loss}}^{-1} \rightarrow 0$ to get a value for τ_n^{-1} alone. Their storage loss rate was as much as a factor of two smaller than measurements from previous experiments. So their measurements were much closer to the true neutron decay rate, greatly reducing the systematic error in the measurements. Also, Serebrov et al. used the neutron lifetime as a unitarity test of the Cabibbo Kobayashi Maskawa (CKM) matrix. The Standard Model of particle physics predicts that the CKM matrix is unitary [9, 10]. The neutron lifetime by Serebrov et al. was in better agreement with this unitarity prediction than the world average lifetime, as shown in Figure 4 of Serebrov et al. [8].

Mathews et al. [11] applied the measurement $Y_p = 0.2452 \pm 0.0015$ from Izotov et al. [12], which is derived from observations of extragalactic HII regions in low metallicity irregular galaxies, to a Standard BBN (SBBN) code [1, 13] available for public download [14]. In the results using the world average neutron lifetime, the above 1σ range of Y_p corresponds to a

range $\eta = 4.8 \pm 0.8 \times 10^{-10}$, not in agreement with the *WMAP* results. Mathews et al. [11] put in the Serebrov et al. lifetime value into the SBBN code [14]. The new lifetime has the effect of lowering Y_p by ≈ 0.0015 for all values of baryon-to-photon ratio η . The 1σ range of η corresponding to $Y_p = 0.2452 \pm 0.0015$ [12] shifts to $\eta = 5.5 \pm 0.9 \times 10^{-10}$. The new range of η is in agreement with the range $\eta = 6.13 \pm 0.25 \times 10^{-10}$ from the *WMAP* measurements.

This article will discuss how the measured isotope abundances and the *WMAP* data constrain parameters from an IBBN cosmology when using the Serebrov et al. neutron lifetime. Various theories of cosmic phase transitions may lead to the formation of baryon inhomogeneous regions, for example during a first order quark hadron phase transition [15, 16, 17, 18] or during the electroweak phase transition [19, 20, 21, 22]. Inhomogeneities can have planar, cylindrical or spherical symmetry. The evolution of baryon inhomogeneous regions can be modelled using an IBBN code (See Lara [6] for a comprehensive list of attempts to model baryon inhomogeneities). The inhomogeneous region is broken up into 64 zones. Within each zone s the time evolution of the number density $n(i, s)$ of isotope species i obeys the following equation [6, 21, 23]

$$\begin{aligned} \frac{\partial n(i, s)}{\partial t} = & n_b(s) \sum_{j, k, l} N_i \left(-\frac{Y^{N_i}(i, s) Y^{N_j}(j, s)}{N_i! N_j!} [ij] + \frac{Y^{N_k}(k, s) Y^{N_l}(l, s)}{N_k! N_l!} [kl] \right) \\ & - 3 \frac{\dot{a}}{a} n(i, s) + \frac{1}{r^p} \frac{\partial}{\partial r} \left(r^p D_n \frac{\partial \xi}{\partial r} \frac{\partial n(i, s)}{\partial \xi} \right). \end{aligned} \quad (2)$$

The first two terms correspond to nuclear reactions and weak decays that create or destroy isotope i within zone s . The weak reactions that interconvert neutrons and protons go in these terms for instance. The third term corresponds to the expansion of the universe. The final term corresponds to diffusion of isotope i between zones. Neutron diffusion is the most prominent diffusion because of the neutrons' lack of charge. The influence of neutron diffusion on IBBN results is described in detail by Lara [6]. Thermonuclear reaction rates from Angulo et al. [24] were used in runs for both Lara [6] and this article.

III. RESULTS

The following results are for a cylindrically symmetric IBBN model with an initial high baryon density in the outermost zones of the model. Parameters used to define the model

include R_ρ , the initial ratio of the high to low baryon densities, and f_v , the volume fraction of the high density region. R_ρ is set to 10^6 , and f_v is defined such that the radius of the low density cylindrical core equals 0.925 of the total radius (the high density outer shell then has a thickness equal to 0.075). This model was used by Orito et al. [25] and by Lara [6, 26] to optimally satisfy the light element abundance constraints and also the inhomogeneous geometry which is calculated in an effective kinetic model of QCD [17]. Final abundance results are presented as contour maps which are dependent on η and the inhomogeneity distance scale r_i , the size of the outermost zone at the initial temperature of 100 GK. For the smallest values of r_i , neutron diffusion homogenizes both neutrons and protons early enough for the resulting abundances to have the same values as abundances from SBBN models.

Note that the code used by Mathews et al. [14] uses Bessel function expansions [1] to solve for the rates of the neutron proton interconversion reactions [27]. The code used in this article uses a numerical integration method to solve for those rates [28]. The difference in the methods of calculating the rates can lead to discrepancies in the value of Y_p on the order of 0.001. There are also differences in the calculation of the Coulomb correction and the zero temperature radiative correction between the codes that affect the results [28, 29]. These differences will be discussed and resolved in a subsequent article.

Figure 1 shows both observational constraints for deuterium in an η vs. r_i contour map and the CMB constraints $\eta = 6.13 \pm 0.25$ from the *WMAP* results [5]. The deuterium observational constraints $D/H = 2.78_{-0.38}^{+0.44} \times 10^{-5}$ are the average of measurements of six absorption-line systems towards five Quasi Stellar Objects [30]. In the SBBN model the deuterium constraints correspond to $\eta = (5.6 - 6.7) \times 10^{-10}$, encompassing the *WMAP* constraints. As can be seen in Figure 1 the results for the smallest values of r_i are equivalent to SBBN results. The bends in the deuterium contour lines are explained in detail in Lara [6]. In models with r_i from ≈ 25000 cm to 10^5 cm, neutron diffusion occurs between weak freeze-out and nucleosynthesis. Contour lines are shifted to lower η (lower deuterium production) because nucleosynthesis is concentrated in regions with large proton density. For r_i from $\approx 10^5$ cm to 2.0×10^6 cm neutron back diffusion does not reach all regions of the model during the time of nucleosynthesis, and contour lines shift instead to higher η (greater deuterium production). At $r_i \approx 2.0 \times 10^6$ cm neutron diffusion peaks at the same time as nucleosynthesis. The deuterium contour lines shift to lower η and the IBBN model is

approximately the average of a high baryon density SBBN model and a low density SBBN model. Due to these bends the deuterium constraints are in concordance with the *WMAP* results for three ranges of distance scale: $r_i \leq 9000$ cm which includes the SBBN case, $r_i = (1.3 - 2.6) \times 10^5$ cm and $r_i = (2.1 - 2.9) \times 10^7$ cm.

Figure 2 shows observational constraints for ${}^4\text{He}$ for the cases of both the world average neutron lifetime and the neutron lifetime by Serebrov et al., along with the deuterium and *WMAP* constraints. Figure 2 shows $Y_p = 0.246$, the 2σ maximum constraint of the measurement 0.242 ± 0.002 by Izotov and Thuan [31]. This measurement is more recent than the previously adopted measurement by Izotov et al. [12]. If the world average neutron lifetime is used $Y_p = 0.246$ corresponds to $\eta = 6.1 \times 10^{-10}$ for the cases of SBBN and IBBN with the smallest values of r_i . Only a very narrow range $\eta = (5.88 - 6.1) \times 10^{-10}$ is then permitted for $r_i \leq 2000$ cm. The region of concordance for $r_i = (1.3 - 2.6) \times 10^5$ cm however is contained within this ${}^4\text{He}$ constraint. Note though that the extent of systematic errors in ${}^4\text{He}$ observations are controversial. Olive and Skillman [32] adopt a conservative approach to accessing uncertainties and report a very large range $0.232 \leq Y_p \leq 0.258$ due to correlated errors. This range should eventually come down as the number of systems with uncorrelated systematic errors increase.

A shorter neutron lifetime means that more neutrons are converted to protons before the onset of nucleosynthesis, and Y_p for a set value of η is smaller. But the lower neutron abundance has no perceptible effect ($< 1\%$) in the final abundances of all other isotopes [11]. Since the neutron lifetime is independent of baryon inhomogeneity, the IBBN run shows the same results. For a set η , Y_p is reduced by 0.0015 while D/H is unchanged, regardless of the value of η or r_i . The contour line of the ${}^4\text{He}$ maximum constraint [31] shifts to higher η by 1×10^{-10} . Using the world average neutron lifetime, the region of concordance between the deuterium and ${}^4\text{He}$ constraints excludes a range $(4.5 \times 10^3 - 1.3 \times 10^5)$ cm of r_i . The shift in the ${}^4\text{He}$ contour line due to the Serebrov et al. lifetime allows for a concordance between deuterium and ${}^4\text{He}$ for all values of $r_i < 6.4 \times 10^5$ cm. The *WMAP* constraints are in concordance with the deuterium constraints and ${}^4\text{He}$ constraints with the Serebrov et al. lifetime for $r_i < 5500$ cm. The region of concordance for $r_i = (1.3 - 2.6) \times 10^5$ cm is still contained within the new ${}^4\text{He}$ constraint. For concordance with the region with $r_i = (2.1 - 2.9) \times 10^7$ cm a maximum value $Y_p = 0.259$ is needed. This value is close to the maximum limit reported by Olive and Skillman, but that maximum limit is expected to

diminish as the errors improve.

The primordial abundance of ^7Li is in dispute because of disagreement over the calculation of the effective temperatures of metal poor halo stars needed to determine the abundances. Ryan et al. [33] and Melendez & Ramirez [34] calculate different values of the effective temperature and different ranges of the ^7Li abundance. Figure 3 shows the Ryan et al. ^7Li constraints $^7\text{Li}/\text{H} = 1.23_{-0.32}^{+0.68} \times 10^{-10}$ along with the deuterium, $WMAP$ and ^4He constraints when using the Serebров et al. lifetime. Figure 4 does the same but instead shows the Melendez & Ramirez constraints $^7\text{Li}/\text{H} = 2.34_{-0.96}^{+1.64} \times 10^{-10}$. Regions of concordance between the ^4He , deuterium, and $WMAP$ constraints are highlighted in yellow (color online).

No region of concordance exists between the ^7Li constraints of Ryan et al. [33] and the constraints from deuterium and ^4He for either the SBBN model or the IBBN model. A depletion factor due to stellar processes is needed for concordance. A factor of 2.5 would bring the ^7Li constraints into concordance with the $WMAP$ constraints $\eta = 6.13 \pm 0.25 \times 10^{-10}$ for the SBBN case and for the IBBN case with distance scale $r_i \leq 2500$ cm. But for $r_i \approx 25000$ cm nucleosynthesis in high proton density regions leads to considerably increased production of ^7Be [6]. The ^7Li contour lines shift to lower η than the contour lines for deuterium and ^4He . Larger depletion factors can then be permitted in the IBBN model. Depletion factors up to 5.9 are permitted using the world average neutron lifetime [6]. The main effect of using the Serebrov et al. lifetime is to shift the ^4He contour lines to higher η . This shift increases the maximum allowed range for the depletion factor, to 9.3 as shown in Figure 3. The constraints by Ryan et al. with this depletion factor will be in concordance with the narrow region $r_i = (1.3 - 2.6) \times 10^5$ cm permitted by the deuterium, ^4He , and $WMAP$ constraints.

Figure 4 shows a thin region of concordance $\eta = (5.88 - 6.0) \times 10^{-10}$ between the $WMAP$ constraints and the 2σ limit of the ^7Li constraints by Melendez & Ramirez [34]. A depletion factor of 1.2 would bring these ^7Li constraints into concordance with the whole range $\eta = 6.13 \pm 0.25 \times 10^{-10}$ of the $WMAP$ constraints for SBBN and for IBBN with $r_i \leq 3000$ cm. Using the world average neutron lifetime a maximum depletion factor of 2.8 of the Melendez & Ramirez constraints is required by this IBBN model [6]. Using the Serebrov et al. neutron lifetime, a maximum depletion factor of 4.47 brings the Melendez & Ramirez constraints with the region $r_i = (1.3 - 2.6) \times 10^5$ cm permitted by the deuterium, ^4He , and $WMAP$ constraints.

The results in this article are for a cylindrically symmetric IBBN model with an initial low density core and high density outer region. Changing the symmetry of the model or changing the values of parameters R_ρ and f_v have the effect of lessening or amplifying the turns in the contour lines, but the characteristics of the contour lines remain the same qualitatively. Contour lines shift to lower η and then to higher η and then back to lower η as the size of the model increases. The particular model of this article is thus representative of IBBN models in general.

We note that new measurements of the ${}^7\text{Li}$ primordial abundance derived from the ratio (${}^7\text{Li}/{}^6\text{Li}$) measured in the interstellar medium [35, 36] support a larger range of permitted depletion factors, consistent with those required here, leaving an enhanced ${}^9\text{Be}$ or ${}^{11}\text{B}$ abundance as a possible observable signature for the IBBN [37, 38, 39].

IV. CONCLUSIONS

We have reanalyzed IBBN in the context of the latest constraints on primordial abundances, input physics, and cosmological parameters. We have shown that some possible IBBN solutions are possible. For example, a cylindrical fluctuation with a comoving radius of $\sim 10^5$ cm fixed at a temperature of 100 GK is still consistent with the D/H, Y_p and WMAP constraints. Depletion factors of up to 9.3 or 4.47, depending on which measurement is used, can bring the ${}^7\text{Li}$ results into concordance as well. Also any fluctuation up to a radius of $\sim 10^4$ cm is viable. Hence, although the standard homogeneous BBN limit is still a consistent and the simplest solution, IBBN remains a viable possibility should it ever be established that such fluctuations arise from earlier cosmic phase transitions.

V. ACKNOWLEDGEMENTS

This work has been supported in part by Grants-in-Aid for Scientific Research (14540271, 17540275) and for Specially Promoted Research (13002001) of the Ministry of Education, Culture, Sports, Science and Technology of Japan, and the Mitsubishi Foundation. This work was also partially funded by National Science Foundation grants PHY 9800725, PHY 0102204, and PHY 035482. Work at UND has been supported under DoE Nuclear Theory grant # DE-FG02-95-ER40934. The authors thank the National Astronomical Observatory

of Japan and their respective academic institutions for the opportunity to carry out this research.

- [1] R. Wagoner, *Astrophys. J.* **179**, 343 (1973).
- [2] J. Yang, M. Turner, G. Steigman, D. Schramm, and K. Olive, *Astrophys. J.* **281**, 493 (1984).
- [3] M. Smith, L. Kawano, and R. Malaney, *Astrophys. J. Suppl.* **85**, 219 (1993).
- [4] A. Melchiorri, in *Dark Matter in Astro- and Particle Physics DARK 2002*, edited by H. Klapdor-Kleingrothaus and R. Viollier (Springer, 2003), p. 101, astro-ph/0204262.
- [5] C. Bennett and et al., *Astrophys. J. Suppl.* **148**, 1 (2003).
- [6] J. Lara, *Phys. Rev. D* **72**, 023509 (2005).
- [7] S. Eidelman and et al [Particle Data Group], *Phys. Lett. B* **592**, 1 (2004).
- [8] A. Serebrov and et al, *Phys. Lett. B* **605**, 72 (2005).
- [9] H. Abele, M. Astruc-Hoffmann, S. Baeßler, D. Dubbers, F. Glück, U. Müller, and V. Nezhevsky, *Phys. Rev. Lett.* **88**, 211801 (2002).
- [10] H. Abele, E. Barberio, D. Dubbers, F. Glück, J. Hardy, W. Marciano, A. Serebrov, and N. Severijns, *Eur. Phys. J. C* **33**, 1 (2004).
- [11] G. Mathews, T. Kajino, and T. Shima, *Phys. Rev. D* **71**, 021302 (2005).
- [12] Y. Izotov, F. Chafhee, C. Foltz, R. Green, N. Guseva, and T. Thuan, *Astrophys. J.* **527**, 757 (1999).
- [13] L. Kawano (1992), fermilab-Pub-92/04-A.
- [14] L. Kawano, available at <http://www-thphys.physics.ox.ac.uk/user/SubirSarkar/bbn.html>.
- [15] H. Kurki-Suonio, *Phys. Rev. D* **37**, 2104 (1988).
- [16] R. Malaney and G. Mathews, *Phys. Rep.* **229**, 145 (1993).
- [17] K. Sumiyoshi, T. Kajino, C. Alcock, and G. Mathews, *Phys. Rev. D* **42**, 3963 (1990).
- [18] E. Witten, *Phys. Rev. D* **30**, 272 (1984).
- [19] G. Fuller, K. Jedamzik, G. Mathews, and A. Olinto, *Phys. Lett. B* **333**, 135 (1994).
- [20] A. Heckler, *Phys. Rev. D* **51**, 405 (1995).
- [21] K. Kainulainen, H. Kurki-Suonio, and E. Sihvola, *Phys. Rev. D* **59**, 083505 (1999).
- [22] A. Mégevand and F. Astorga, *Phys. Rev. D* **71**, 023502 (2005).
- [23] G. Mathews, B. Meyer, C. Alcock, and G. Fuller, *Astrophys. J.* **358**, 36 (1990).

- [24] C. Angulo and et al., Nucl. Phys. A **656**, 3 (1999).
- [25] M. Orito, T. Kajino, R. Boyd, and G. Mathews, Astrophys. J. **488**, 515 (1997).
- [26] J. Lara, in *Frontier in Astroparticle Physics and Cosmology*, edited by K. Sato and S. Nagataki, Research Center for the Early Universe (Universal Academy Press, 2004), p. 87, astro-ph/0402112.
- [27] S. Weinberg, *Gravitation and Cosmology* (John Wiley and Sons Inc., 1972), p. 547.
- [28] J. Lara, Ph.D. thesis, University of Texas at Austin (2001).
- [29] D. Dicus, E. Kolb, A. Gleeson, E. Sudarshan, V. Teplitz, and M. Turner, Phys. Rev. D **26**, 2694 (1982).
- [30] D. Kirkman, D. Tytler, N. Suzuki, J. O'Meara, and D. Lubin, Astrophys. J. Suppl. **149**, 1 (2003).
- [31] Y. Izotov and T. Thuan, Astrophys. J. **602**, 200 (2004).
- [32] K. Olive and E. Skillman, Astrophys. J. **617**, 29 (2004).
- [33] S. Ryan, T. Beers, K. Olive, B. Fields, and J. Norris, Astrophys. J. **530**, L57 (2000).
- [34] J. Melendez and I. Ramirez, Astrophys. J. **615**, L33 (2004).
- [35] S. Kawanomoto, T.-K. Suzuki, H. Ando, and T. Kajino, Nucl. Phys. A **718**, 659 (2003).
- [36] S. Kawanomoto and et al. [SUBARU/HDS Collaboration] (2005), submittal to Astrophys. J.
- [37] R. Boyd and T. Kajino, Astrophys. J. **336**, L55 (1989).
- [38] R. Malaney and W. Fowler, Astrophys. J. **345**, L5 (1989).
- [39] T. Kajino and R. Boyd, Astrophys. J. **359**, 267 (1990).

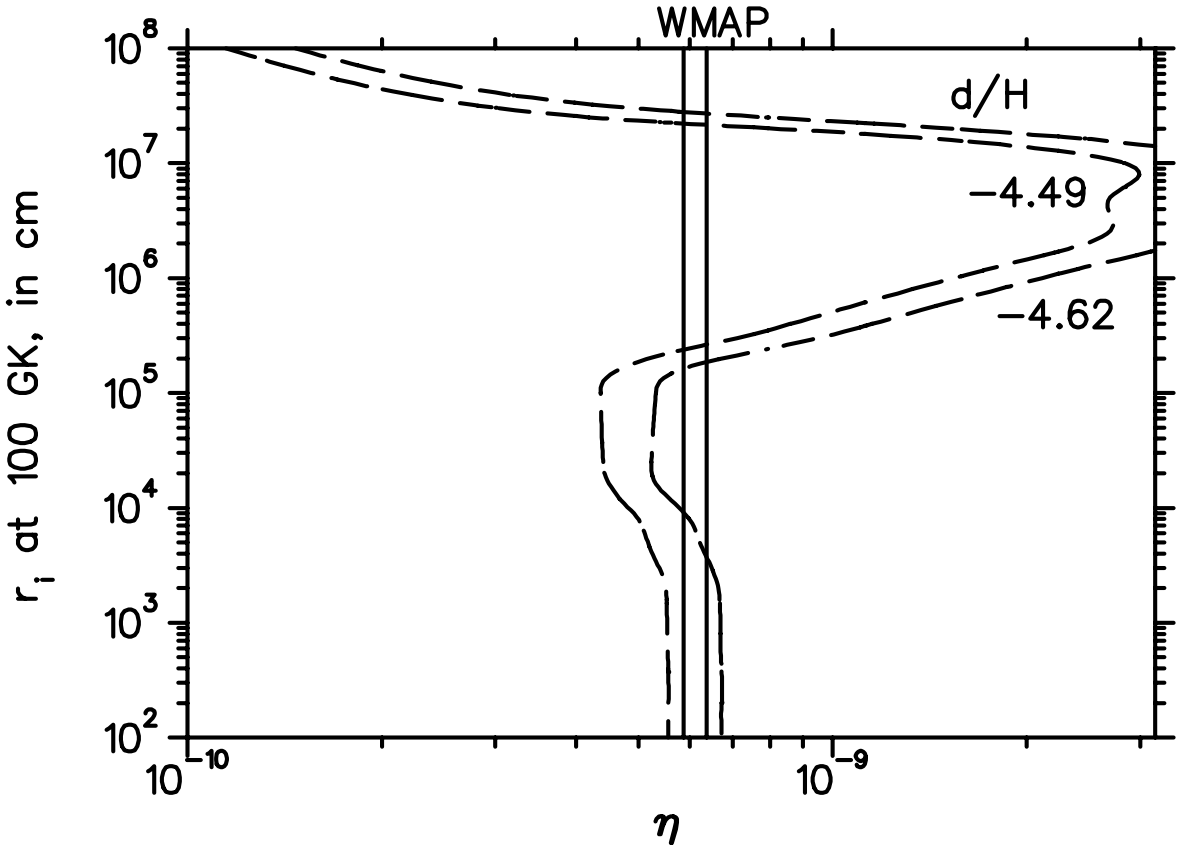


FIG. 1: Contours consistent with the $\pm 2\sigma$ measured abundance ratio D/H of deuterium [30] are shown in long dashed lines. The CMB constraints from the *WMAP* measurements [5] are also shown as solid lines. The *WMAP* constraint limits the allowed parameter space to three regions.

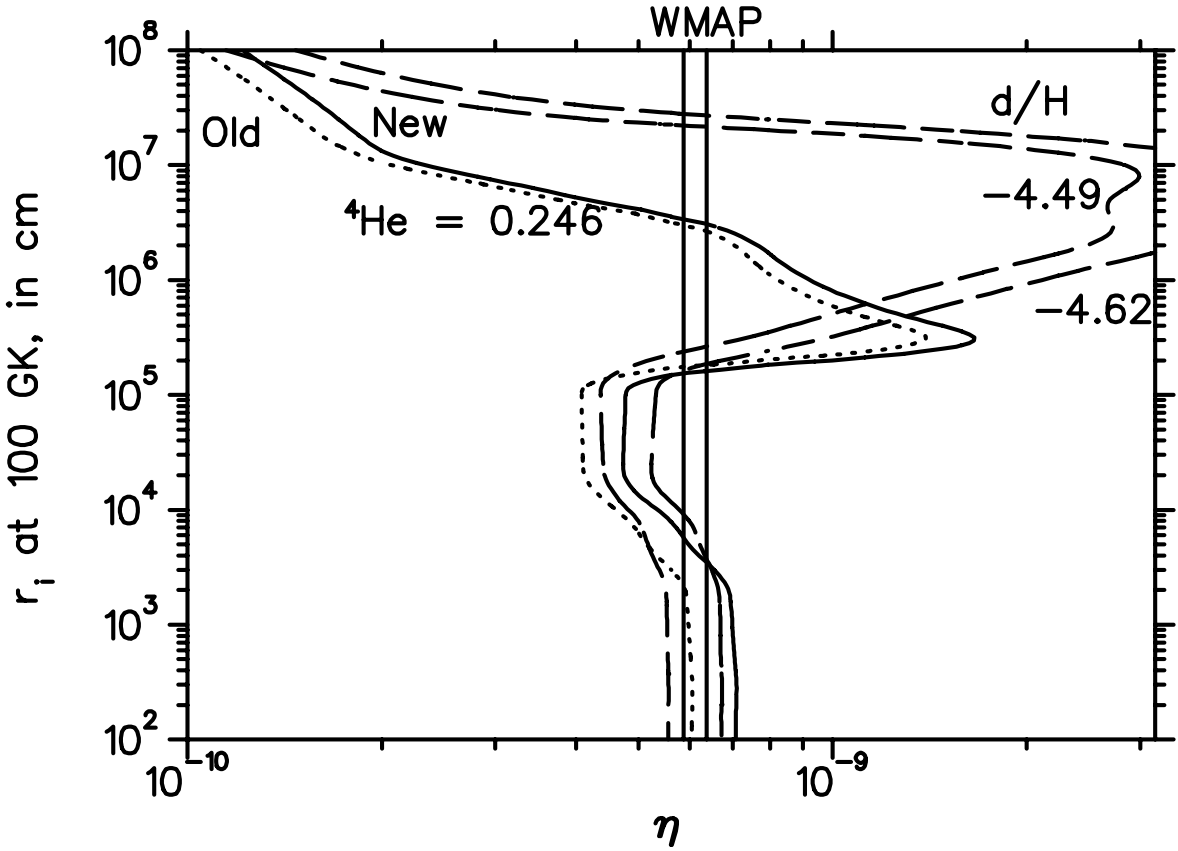


FIG. 2: Constraints from deuterium and CMB observations are shown with the $+2\sigma$ maximum constraint of the ${}^4\text{He}$ mass fraction Y_p by Izotov and Thuan [31]. The contour for the $+2\sigma$ maximum constraint of Y_p is shown by dashed line for the world average neutron lifetime [7] and solid line for the Serebrov et al. lifetime [8]. The region to the right of the maximum constraint is excluded. The $+2\sigma$ minimum constraint corresponds to values of η so low it is not necessary to show in this figure. The lifetime effect is to shift the Y_p contour line to a higher η by $\approx 1 \times 10^{-10}$.

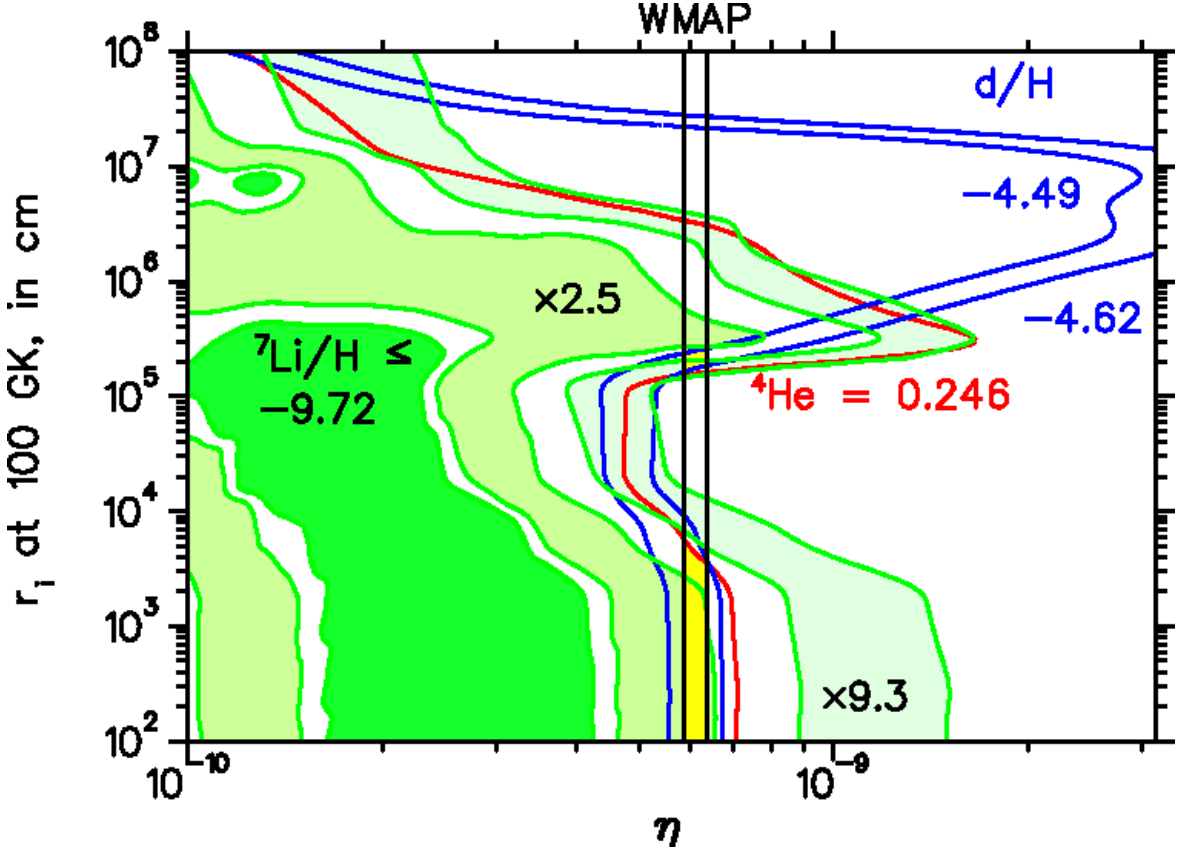


FIG. 3: (Color Online) Contours for the $\pm 2\sigma$ abundance constraints on ${}^7\text{Li}/\text{H}$ by Ryan et al. [33] are shown along with the constraints on deuterium [30], CMB constraint from *WMAP* [5], and $+2\sigma$ maximum constraint on ${}^4\text{He}$ [31] for the case of $\tau_n = 878.5 \pm 0.7_{\text{stat}} \pm 0.3_{\text{sys}}$ [8]. The region of concordance between *WMAP*, ${}^4\text{He}$ and deuterium is shown in yellow. The contour lines for ${}^7\text{Li}$ allow for depletion factors from 2.5 to 9.3 to bring all three observational constraints and CMB constraints in concordance with each other.

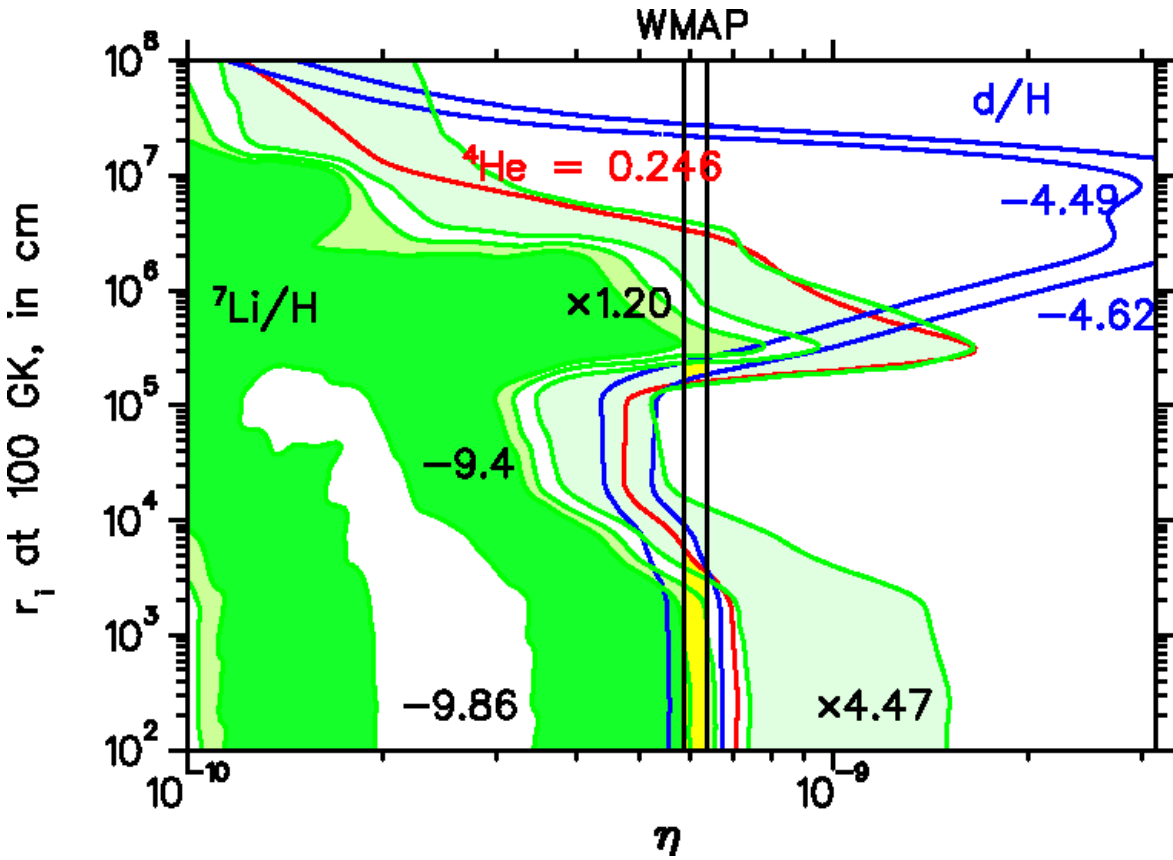


FIG. 4: (Color Online) Same as in Figure 3 but with $\pm 2\sigma$ constraints on ${}^7\text{Li}/\text{H}$ by Melendez & Ramirez [34]. A thin region of concordance between the $\pm 2\sigma$ limit of the ${}^7\text{Li}$ constraints and the other constraints exists for $r_i \leq 1000$ cm. A depletion factor of 1.2 improves concordance. A depletion factor of 4.47 would bring these ${}^7\text{Li}$ measurements in concordance with the other constraints for $r_i = (1.3 - 2.6) \times 10^5$ cm.